Effects of CO2 on P-wave attenuation in porous media with micro-cracks: A synthetic modelling study

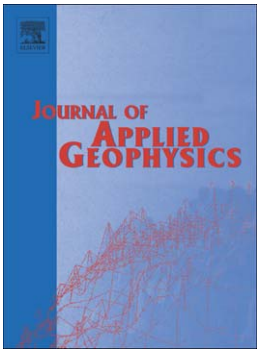

Effects of CO_2 on P-wave attenuation in porous media with micro-cracks: A synthetic modelling study

A.M. Ekanem, X.Y. Li, M. Chapman, I.G. Main

PII: S0926-9851(16)30449-9
DOI: doi:10.1016/j.jappgeo.2016.10.025
Reference: APPGEO 3112

To appear in: *Journal of Applied Geophysics*

Received date: 19 March 2015
Revised date: 11 August 2016
Accepted date: 27 October 2016

Please cite this article as: Ekanem, A.M., Li, X.Y., Chapman, M., Main, I.G., Effects of CO_2 on P-wave attenuation in porous media with micro-cracks: A synthetic modelling study, *Journal of Applied Geophysics* (2016), doi:10.1016/j.jappgeo.2016.10.025

Effects of CO_2 on P-wave attenuation in porous media with micro-cracks: a synthetic modelling study

Ekanem, A. M.[1, 2, 3]; Li, X. Y.[3, 4], Chapman, M.[2, 3] and Main, 1. G.[2]

*[1] Department of Physics, Akwa Ibom State University, Mkpat Enin, Nigeria (**current address**)*
[2] School of Geosciences, University of Edinburgh, EH9 3JW, UK
[3] British Geological Survey, Murchison House, Edinburgh, EH9 3LA, UK
[4] CNPC Geophysical Key Laboratory, China University of Petroleum, Beijing, China

Email address: anny4mart@yahoo.com

Abstract

The presence of CO_2 in hydrocarbon reservoirs can cause significant changes in seismic wave properties. In turn these properties can be used to map CO_2 saturation in hydrocarbon reservoirs or aquifers - either from natural sources or by injection from the surface. We present the results of a synthetic modelling study of the effects of supercritical CO_2 saturation on P-wave attenuation in a medium consisting of four horizontal layers, including a target aquifer. The target aquifer is modelled fully by an effective medium containing pores saturated with brine and/or CO_2 and randomly-aligned microcracks at different densities. The other layers are modelled solely by their bulk seismic velocities and densities. We first compute synthetic seismograms for a reference case where the third layer is completely isotropic with no cracks, no pores and no fluid saturation. We then calculate synthetic seismograms for finite crack densities of 0.01, 0.02 and 0.03 at varying degrees of CO_2 saturation in the third layer. The results of our analysis indicate that attenuation is sensitive both to CO_2 saturation and the crack density. For a given crack density, attenuation increases gradually with decreasing percentage of CO_2 saturation and reaches a maximum at around 10 % saturation. The induced attenuation increases with crack density and with offset. These observations hold out the potential of using seismic attenuation as an additional diagnostic in the characterisation of rock formations for a variety of applications, including hydrocarbon exploration and production, subsurface storage of CO_2 or geothermal energy extraction.

Keywords: Attenuation, Seismic Quality Factor, CO_2, microcracks, fluid saturation

1.0 Introduction

CO_2 is a natural constituent of hydrocarbon reservoirs with saturations varying from 2 - 80% (Roberts, 2009). It is also often deliberately injected into hydrocarbon reservoirs to enhance production rates and sweep efficiencies, and stored in subsurface reservoirs and saline aquifers as a means of mitigating climate change from the burning of fossil fuels. At surface temperatures and pressures, CO_2 exists in the gaseous phase but exhibits supercritical behaviour above the critical point: temperature Tc = 31.1^{o}C and pressure Pc = 7.38 MPa (David *et al*, 2008). White (1975) demonstrated that the presence of a gas in the rock can have a substantial influence on the seismic wave velocity and attenuation, depending on the degree of saturation, permeability, frequency and porosity. The presence of CO_2 in the reservoir either in the gaseous or supercritical state can cause significant changes in seismic properties (such as seismic wave travel time, velocity, amplitude, attenuation) and thus, an understanding of its influence could be of great importance in the study of hydrocarbon reservoir properties. For instance, Davis *et al.* (2003) reported that CO_2 can cause a change of 4 - 6% in P-wave velocity and 5 - 10% in S - wave velocity. Time - lapse studies for monitoring CO_2 sequestration in the subsurface have also shown that the presence of CO_2 can cause significant changes in both the P - and S - wave velocities (e.g. Arts *et al.*, 2004; Chadwick *et al.*, 2005, Amir and Landro, 2009). David *et al.* (2008) observed significant changes in the calculated bulk seismic velocity and density in CO_2 - saturated porous reservoir rocks under field conditions, where the CO_2 may exist either as a supercritical fluid or as a supercritical gas. In both cases, the bulk density decreases systematically and linearly with increasing percentage of CO_2 saturation, though more distinctly for the supercritical gas case. Their results demonstrate that the P-wave velocity shows an obvious non-linear

relationship with saturation. For the supercritical fluid case, there is a remarkable decrease in the P-wave velocity between zero and 30 % CO_2 saturation and thereafter very little or no change in the velocity. For the supercritical gas case, there is even a stronger decrease in the P-wave velocity at small CO_2 saturations of < 5 - 10 % with very little or no change at higher saturations.

The attenuation of seismic wave energy in rocks depends on the physical state of the rocks and on the degree and type of fluid saturation in the pore space. For instance, P-wave attenuation has been shown to be greater in partially-saturated rocks compared to fully-saturated rocks (e.g. White, 1975; Toksoz *et al.*, 1979; Johnson *et al.*, 1979; Winkler and Nur, 1982; Klimentos, 1995). Despite the intensive effort in research and development related to the effects that CO_2 might have on seismic wave response (e.g. Rubino *et al.,* 2011a and Rubino *et al.*, 2011b, Rossi *et al.*, 2011, Müller *et al., 2015*), there is still a lack of adequate understanding of the effects of CO_2 on seismic wave attenuation, especially at varying degrees of saturation. Thus, a concerted effort is still needed for a fuller understanding of these complex processes. In this paper, we examine the effects of CO_2 held in the pore space of the rock on seismic attenuation, through synthetic modelling. To provide a realistic scenario for the modelling study, we use the published bulk moduli of both brine and CO_2 measured in the Sleipner gas field in the North Sea (Chadwick *et al.*, 2005). Our main aim is to examine the changes caused by the presence of CO_2 at varying percentages of saturation on P - wave attenuation in a layered medium where the target layer contains randomly-aligned microcracks. Our theoretical model consists of four horizontal isotropic layers, where the third layer is the target layer. The layer is modelled as a fully poro-elastic medium containing brine with different crack densities and different amounts of injected CO_2. The model accounts for anelastic losses due to the squirt-flow mechanism, which in turn depends on the crack density and fluid properties. To simplify the treatment, we assume the other layers can be characterised solely by their isotropic bulk velocities and densities. We first

calculate a reference model for the case that the third layer has zero crack density, no pores and no fluid saturation. We then consider a case in which the third layer in the model is saturated with CO_2 at concentrations varying from 0 to 100 % and crack densities of 0.01, 0.02 and 0.03 respectively. We used the classical spectral ratio method to compute the induced attenuation from the synthetic data. Our results demonstrate the sensitivity of attenuation to CO_2 saturation, providing a fuller understanding into the effects of the pattern of seismic attenuation caused by CO_2 in fluid-saturated porous rocks and especially validating the practical utility of using attenuation characteristics as an additional diagnostic in the characterisation of rock formations for a variety of applications, including hydrocarbon exploration and production, subsurface storage of CO_2 or geothermal energy extraction.

2.0 Chapman's poro-elastic model

The poro-elastic model of Chapman (2003) considers the pore space of a rock to consist of a lattice configuration of spherical pores, randomly oriented ellipsoidal micro-cracks and aligned ellipsoidal fractures. The radius of the micro-cracks and spherical pores is identified with the grain size. The fracture size is assumed to be much larger than the grain size but smaller than the seismic wavelength. Since the fractures have preferential alignment, the resulting medium has hexagonal symmetry (transverse isotropy). Wave-induced pressure gradients cause fluid exchange between adjacent elements of pore space in the rock. The fluid exchange between two adjacent voids 'a' and 'b' for instance is described by the formula (Chapman 2003):

$$\partial_t \mathrm{m_a} = \frac{\rho_o \kappa \varsigma}{\eta}\left(\mathrm{p_b} - \mathrm{p_a}\right) \tag{1}$$

where ρ_o is the fluid density, κ is the permeability, ς is the grain size, η is the fluid viscosity, $\mathrm{p_a}$ is the pressure in element a, $\mathrm{m_a}$ is the mass of fluid in element a and $\mathrm{p_b}$ is the pressure in element b. Each element of pore space is assumed to be connected to six other

elements and the resulting flows can be added linearly. The fractures are connected to a greater number of elements since they are larger than the micro-cracks and the pores. For the purpose of ensuring that there is some spacing between the fractures, the model assumes that each micro-crack or pore is connected to at most one fracture and that the fractures are not connected to each other. These last assumptions require that the number of micro-cracks and pores greatly exceeds the number of fractures. The effective elastic tensor, *C* given by Chapman (2003) is of the form:

$$\mathbf{C} = \mathbf{C}^{(0)} - \phi_{\mathrm{p}}\mathbf{C}^{(1)} - \varepsilon_{\mathrm{c}}\mathbf{C}^{(2)} - \varepsilon_{\mathrm{f}}\mathbf{C}^{(3)} \tag{2}$$

where $\mathrm{C}^{(0)}$ is the elastic tensor of the isotropic rock matrix with Lame's parameters λ and μ, $\mathrm{C}^{(1)}$, $\mathrm{C}^{(2)}$ and $\mathrm{C}^{(3)}$ are the additional contributions from pores, micro-cracks and fractures, respectively, multiplied by the porosity ϕ_{p}, the crack density ε_{c} and the fracture density ε_{f}. These additional contributions are functions of the Lamé parameters, fluid and fracture properties, frequency and relaxation times associated with squirt flow.

Chapman's (2003) original model is restricted to very low porosity since the elastic constants are calculated based on Eshelby's (1957) interaction energy approach which is only valid for dilute concentrations of inclusions (Maultzsch *et al.*, 2003). In cases of high porosities, the calculation of the corrections using the grain moduli λ and μ might result in significant errors. Furthermore, it is not ideal to use moduli which cannot be obtained from measured velocities. To address these issues, Chapman *et al.* (2003) slightly adapted the model to make it more applicable to real data by using Lame's parameters λ^o and μ^o derived from the density ρ and measured P-wave velocity V_p^o and S-wave velocity V_s^o of the un-fractured rock for the corrections. Also, $\mathrm{C}^{(0)}(\Lambda, \mathrm{M})$ is defined in such a way that the measured isotropic velocities are obtained by applying the pore and crack corrections at a specific frequency f_o (Chapman *et al.,* 2003 and Maultzsch *et al*., 2003). Thus:

$$\Lambda = \lambda^{o} + \phi_{c,p}\left(\lambda^{o},\mu^{o},f_{o}\right), \quad M = \mu^{o} + \phi_{c,p}\left(\lambda^{o},\mu^{o},f_{o}\right), \tag{3}$$

where $\phi_{c,p}$ refers to corrections to the elastic tensor which are proportional to crack density and porosity.

$$\lambda^{o} = \rho\left(V_{p}^{o}\right)^{2} - 2\mu^{o}\ ; \quad \mu^{o} = \rho\left(V_{s}^{o}\right)^{2} \tag{4}$$

Equation 2 can then be re-written as:

$$C = C^{(0)}(\Lambda, M, \omega) - \phi_{p}C^{(1)}\left(\lambda^{o}, \mu^{o}, \omega\right) - \varepsilon_{c}C^{(2)}\left(\lambda^{o}, \mu^{o}, \omega\right) - \varepsilon_{f}C^{(3)}\left(\lambda^{o}, \mu^{o}, \omega\right) \tag{5}$$

The form of Equation 5 allows the corrections for pores, micro-cracks and fractures which describe the frequency dependence and anisotropy of a material to be obtained from measurements of the velocities (Maultzsch *et al.*, 2003). Chapman *et al.* (2003) further simplified the model by setting the crack density to zero in the case of high porosity. The influence of this parameter however is not significant for modelling the effects of fractures provided the spherical porosity is much greater than the crack porosity (Maultzsch *et al.*, 2003).

Fluid flow in Chapman's (2003) model occurs at two scales; the grain scale (associated with the micro-cracks and spherical pores) and the fracture scale. This results in two characteristic frequencies and corresponding relaxation times. The relaxation time, τ_{m} associated with fluid flow between the micro-cracks and spherical pores are related to the squirt-flow frequency, f_{m}^{c} as (Murphy, 1985; Winkler, 1986; Lucet and Zinszner, 1992; Sothcott *et al.*, 2000):

$$f_{m}^{c} = \frac{1}{\tau_{m}} \tag{6}$$

$$\tau_{m} = \frac{c_{v}\eta\left(1 + K_{c}\right)}{\sigma_{c}\kappa\varsigma_{1}}, \tag{7}$$

where c_v is the volume of an individual crack, σ_c is the critical stress and c_1 is the number of connections to other voids. σ_c and K_c are defined by:

$$\sigma_c = \frac{\pi \mu r}{2(1-\nu)} \tag{8}$$

$$K_c = \frac{\sigma_c}{\kappa_f} \tag{9}$$

where r is the aspect ratio of the cracks, v is the poison's ratio of the matrix and κ_f is the fluid bulk modulus. Fluid flow in and out of the fractures is associated with a lower characteristic frequency or a higher corresponding relaxation time τ_f which is dependent on the size of the fractures. The relaxation time associated with the grain scale and that associated with the fracture scale are both related by the equation (Chapman, 2003):

$$t_f = \frac{a_f}{\varsigma} \tau_m \tag{10}$$

where a_f is the fracture radius. From Equation 10, it can be inferred that larger fractures will result in higher relaxation times (or lower characteristic frequencies). These larger relaxation times lead to velocity dispersion and attenuation in the seismic frequency range. Thus, in the general case the resulting anisotropy is frequency dependent.

2.0 Theoretical model and experimental set-up

The theoretical model is made up of four horizontal isotropic layers (Figure 1). To investigate the effects of CO_2, a porous fluid-saturated material is introduced into the third layer and squirt flow between the pores in the matrix is taken into consideration. The material is saturated with brine and CO_2 (in the supercritical state) at different degrees of concentrations. The elastic properties of the porous material are computed using the poroelastic model of Chapman (2003). However, to model the effect of fluid saturation in a porous but un-fractured medium, we set the fracture density to zero so that the model returns to the earlier

model of Chapman *et al.* (2002). The bulk moduli of the brine and CO_2 are based on the data from the Sleipner field in the North Sea (Chadwick *et al*., 2005). The field is a site for large scale CO_2 injection project specifically designed as a greenhouse gas mitigation measure (Chadwick *et al*., 2005). Millions of tonnes of CO_2 have been injected since 1996 into the Utsira Sand, which constitutes a major saline aquifer in the field (Chadwick *et al.*, 2005; Bickle *et al.*, 2007; Arts, *et al.*, 2008) with over 11 million tonnes by 2010 (Chadwick *et al.*, 2010). The Utsira sand has a thickness of 200 - 300m and CO_2 exists in the reservoir in the supercritical phase (Chadwick *et al*., 2005). Details of the model parameters used are given in Table 1.

A uniform saturation of the pores and cracks with two types of fluids (brine and CO_2 in this case) will result in a change of the effective fluid bulk modulus, viscosity and density (Chapman and Liu 2006 and David *et al.*, 2008). The resulting attenuation is sensitive to the changes in the effective fluid bulk modulus as well as the fluid viscosity (Chapman and Liu, 2006; Maultzsch *et al.,* 2007). For partial saturation conditions with homogeneous mixing of brine and CO_2, the effective fluid bulk modulus K_{eff} could be computed using Wood's formula as (Mavko *et al*., 2009, pp 282):

$$\frac{1}{K_{eff}} = \frac{S_w}{K_w} + \frac{1 - S_w}{K_c} \tag{11}$$

where K_w is the bulk modulus of brine, K_c is the bulk modulus of CO_2 and S_w is the percentage of brine saturation. Wood's formula is valid for the low frequency limit, where there is sufficient time for fluid pressure gradients to relax and equilibrate to a constant pressure. The equilibrium is reached due to the fact that only grain scale is considered in the model where the relaxation times are much smaller than those expected if fractures were to be present. The pressure gradient generated by a seismic wave propagating in a medium leads

to exchange of fluid between the microcracks and the surrounding pore space, resulting in attenuation. This attenuation is sensitive to the fluid effective modulus in this case.

Firstly, we considered a pure isotropic model with zero porosity, no fluid saturation and no microcracks to provide a reference model and computed the synthetic data from the theoretical model using the 'ANISEIS' software which makes use of the reflectivity method (Taylor, 2001). Aniseis is a commercial software package for modelling seismic wave propagation in anisotropic media and is a far field approximation. We then introduced brine and CO_2 (in the supercritical state) into the third layer at 90 % and 10 % respectively for crack densities of 0.01, 0.02 and 0.03 to examine the attenuation effects caused by CO_2 on the P-waves generated. We finally examined the sensitivity of the induced attenuation to CO_2 saturation by considering the case in which the third layer is saturated with brine and CO_2 at different degrees of concentrations ranging from 0 to 100 %. A zero percent (0 %) CO_2 saturation implies that the material is fully saturated with brine while 100 % CO_2 saturation means that the material is fully saturated with CO_2. The effective fluid bulk moduli of the fluid saturation were computed using Equation 11. At lower brine saturation, the effective fluid bulk modulus is dominated by the bulk modulus of CO_2. The reverse is the case at higher brine saturation.

A Ricker wavelet with a centre frequency of 25 Hz and a start time of 100 ms was used as the source wavelet. The resulting wavefield was calculated at some 21 positions at the surface of layer 1, at a regular spacing of 100 m, and a minimum source - receiver spacing of 100 m was maintained. The synthetic data were recorded with a time step of 1 ms and a total sampling time of 3 s. Sample synthetic gathers are shown in Figure 2 with the reflections from the top and bottom of the third layer highlighted by the red and green arrows respectively. These reflections are proportional to the time derivative of the source Ricker wavelet. The very low amplitude hyperbolic event that arrives after the reflection from the bottom of the third layer

is the P-S converted wave which was not analysed in this work. There is no significant difference between Figures 2a and b as a result of the auto scaling of the software used in generating the plots. The software scales the amplitude based on the maximum amplitude on the first trace in the gather. Our modelling studies examine only the fluid bulk modulus effect and the effect of viscosity is not considered at this stage.

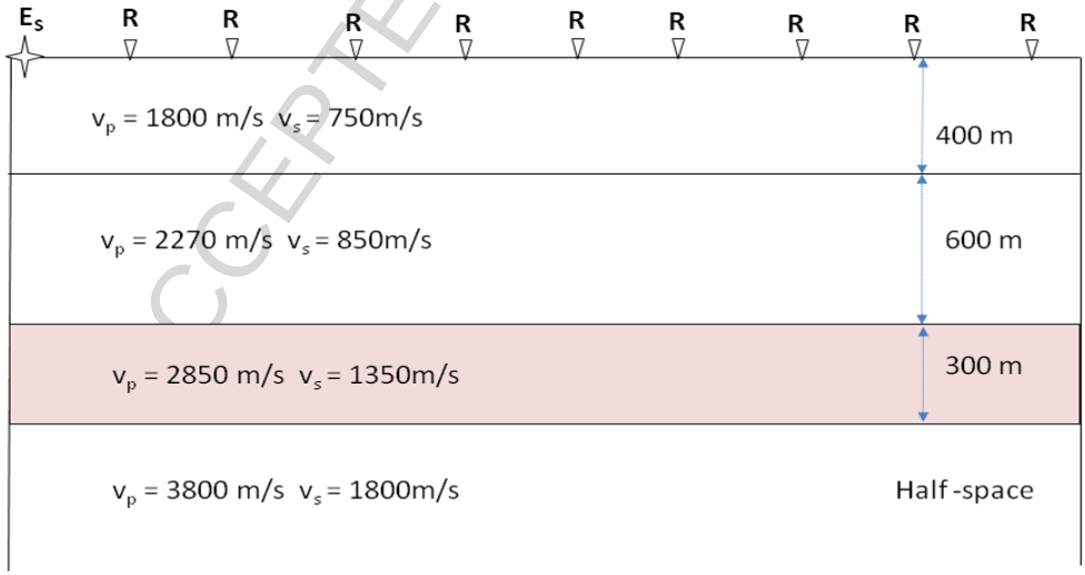

Figure 1: Experimental set-up. The model comprises four horizontal layers. E_S is the source placed at a distance of 100 m from the first receiver R. The receiver spacing is 100 m.

Table 1: Theoretical model parameters

Layer parameters	saturated layer parameters (layer 3)

Layer	v_p (m/s)	v_s (m/s)	ρ (Kg/m^3)	Thickness (m)
1	1800	750	1100	400
2	2270	850	2100	600
3	2850	1350	2450	300
4	3800	1800	2600	Half-space

fracture density	0
CO_2 bulk modulus	0.008Gpa
Brine bulk modulus	2.305Gpa
porosity	0.37

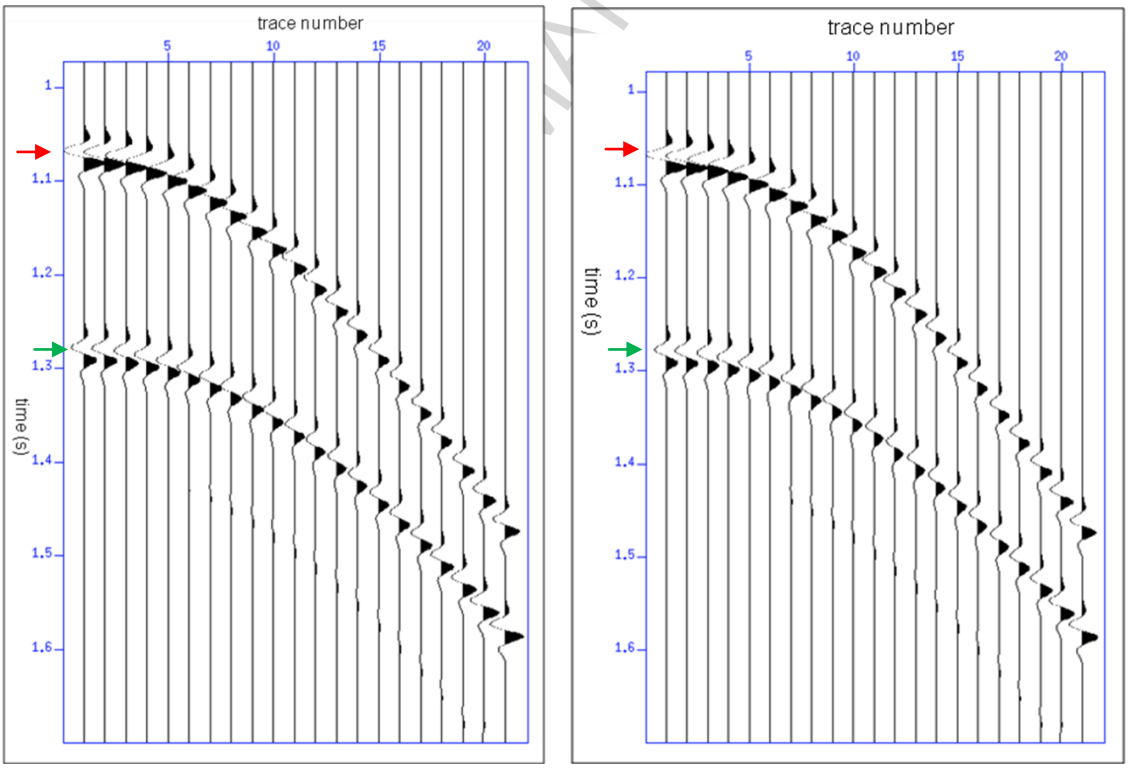

(a) (b)

Figure 2: Sample synthetic data (a) pure isotropic model with no cracks and no fluid saturation (b) model with crack density 0.01 and CO_2 saturation 10% in the third layer. The red and green arrows indicate the top and bottom of the third layer reflections respectively. The trace spacing is 100 m

3.0 Attenuation measurements

Measurement of seismic attenuation from seismic data is usually made through the estimation of the inverse of the seismic quality factor, Q. In practice, the use of the spectral ratio method

is very common to estimate Q from seismic data partly as a result of its ease of use and stability (e.g. Hauge 1981; Pujol and Smithson 1991; Dasgupta and Clark 1998), and also because it removes the effects of geometric spreading in an uncomplicated manner. Consequently, any measurement of attenuation can be attributed exclusively to internal energy dissipation or 'intrinsic attenuation', at least for relatively uniform media where multiple scattering can be neglected.

In this paper, we used the spectral ratio method to estimate the seismic quality factor from the synthetic data. In each gather, the first trace from the top model reflection at an offset of 0 m was used as the reference trace for comparison of the spectral ratios. For each trace in the gather and for the top and bottom reflections from the third layer (fluid-saturated layer), we formed the spectral ratios in accordance with Equation 12 and performed a simple least-squares regression of the Log of the Power Spectral Ratios (LPSR) against frequency. We used a constant FFT time window of 180 ms to compute the power spectra.

$$\ln\frac{A_2^{\,2}}{A_1^{\,2}} = \ln\frac{P_2}{P_1} = 2\ln(R_e G) - \frac{2\pi f}{Q}(t_2 - t_1) \qquad 12$$

f is frequency, R_e is the reflectivity term, G is the geometrical spreading factor, A_1 is the spectral amplitude of the reference trace i.e. for the case of zero crack density, A_2 is the spectral amplitude of the target reflection (top or bottom of fractured-layer) while P_1 and P_2 are the respective spectral powers (square of amplitudes), t_1 and t_2 are the corresponding travel times, Q is the seismic quality factor down to the reflector.

Sample power spectra are shown in Figure 3 for selected percentages of CO_2 saturation and crack density of 0.02 at a fixed offset of 900 m. There is a significant drop in the power spectral density for the bottom layer reflection with decreasing percentage of CO_2 saturation from 100% to a minimum at 10% saturation. However, the power density is a maximum at

0% CO_2 saturation when the material is 100% saturated with brine. These observations are indicative of the sensitivity of the wave attenuation to the varying degrees of CO_2 saturation. The far field pulse shape is proportional to the time derivative of the input Ricker wavelet. Lange and Almoghrabi (1988) and Chung and Lawton (1995) have shown that given a Ricker wavelet with centre frequency f_o, the peak frequency f_p of the derivative of the wavelet is given as:

$$f_p = f_o\sqrt{\frac{3}{2}} \tag{13}$$

Equation 13 explains why the peak frequency of the far field response is greater than that of the input Ricker wavelet. Samples plots of the Log Power Spectral Ratios (LPSR) against frequency are shown in Figure 4 for the pure isotropic model with no fluid saturation and crack density and for 10 % CO_2 saturation and crack density of 0.01 respectively. For the top layer reflection (red colour), the plots are approximately horizontal, indicating that there is no attenuation in the overlying layer (layer 2) as expected since it is isotropic. For the pure isotropic model with no fluid saturation (Figure 4a), the plot for the bottom reflection (blue colour) is also horizontal indicating no attenuation in the model. However, this is not the same for the fluid saturated case (Figure 4b). The plot for the bottom layer is not horizontal, indicating that attenuation is induced by the saturated CO_2. Figure 5 shows sample plots of the Log Power Spectral Ratios (LPSR) against frequency for the third layer for the three values of crack densities considered at 10% CO_2 saturation (Figure 5a) and various degrees of CO_2 saturation at crack density of 0.02 (Figure 5b) at 1100m offset. For the top layer reflection (blue colour), the plots are horizontal, indicating that there is no attenuation in the overlying layer. However, for the three crack densities, the plot for the bottom layer has varying slopes indicating varying magnitudes of attenuation respectively with crack density of 0.03 having the highest magnitude. Also, the plots for the bottom layer reflections for the

various degrees of saturation considered have varying slopes with 10% saturation having the highest slope, implying varying attenuation magnitudes in the layer with highest magnitude at 10% saturation. All the plots however are approximately linear between the frequency bandwidth of 20 - 90 Hz. This frequency bandwidth was used for all the traces analysed. Sample least-squares regression plots of the LPSR against frequency for the chosen bandwidth are shown in Figure 6 for the top (blue colour) and bottom (red colour) reflections from the third layer at selected percentages of CO_2 saturation and a fixed offset of 1100 m respectively with their corresponding coefficient of determination **(**R^2) values. The plots show good fit of the spectral ratios, indicating a linear relationship as predicted by Equation (12) even though attenuation is frequency dependent in the model (Equation 10). The plot for 0 % CO_2 saturation has a slope which is less than that for 100 % CO_2 saturation, indicating that CO_2 causes more attenuation than brine.

We then computed the Q value down to the reflector for a given offset from the slope p of the least-squares regression given by:

$$p = -\frac{2\pi(t_2 - t_1)}{Q} \tag{14}$$

This model assumes Q is frequency-independent. While this is not the case for the model used to construct the synthetic medium, it provides a good approximation to the synthetic data within the restricted bandwidth used in the regression fit. With the pair of Q values computed for the top and bottom of the third layer, we used the layer-stripping method of Dasgupta and Clark (1998) to compute the interval Q_i value in the layer using the equation:

$$Q_i = \frac{[t_2 - t_1]}{t_2/Q_2 - t_1/Q_1} \tag{15}$$

where Q_1 and Q_2 are the seismic quality factors down to top and bottom of the third layer respectively. The entire procedure was repeated for all the traces in the gather following the hyperbolic travel path and the average interval Q in the third layer was computed from the mean of all the computed interval Q_i values in the layer.

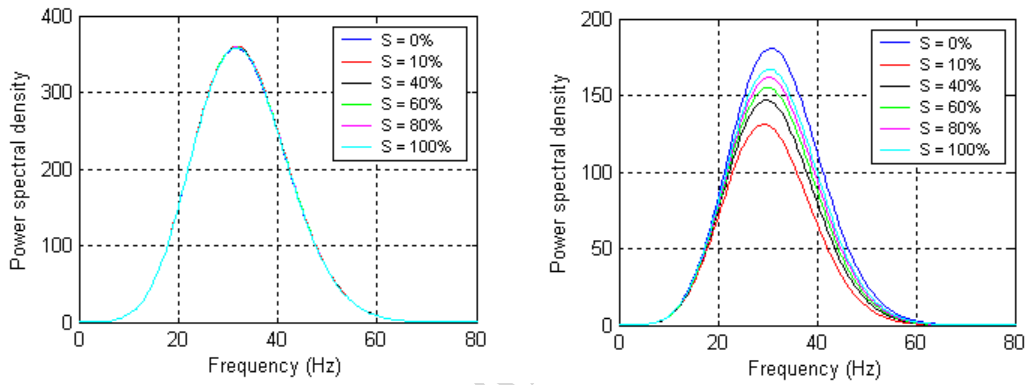

Figure 3: Power spectra at 900 m offset for the fluid-saturated layer reflections (a) top layer: 0.02 crack density (b) bottom layer: 0.02 crack density. S is the degree of saturation of CO_2. The saturation of brine is (100 - S) %.

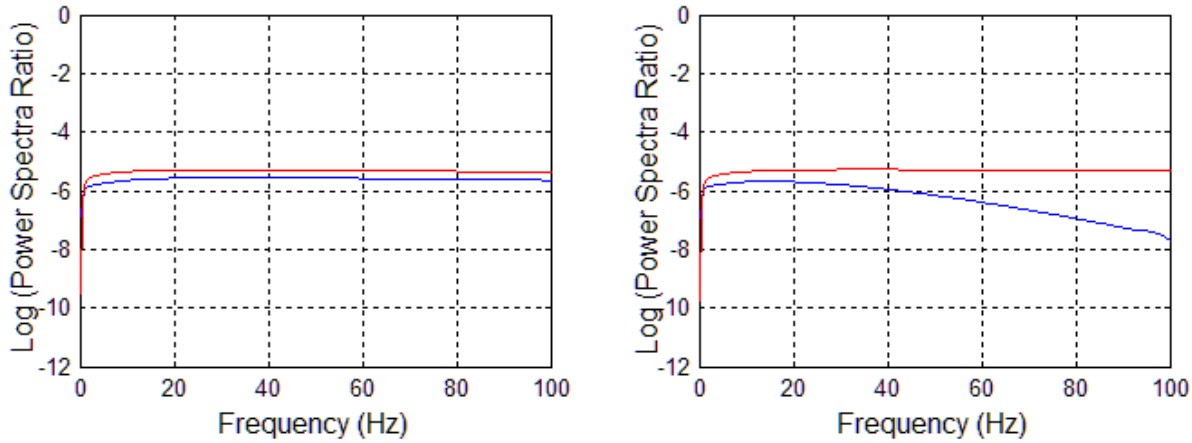

Figure 4: Samples plots of the Log Power Spectral Ratios (LPSR) against frequency at a fixed offset of 1100 m for the third layer (a) zero porosity, no fluid saturation and no microcracks or fractures (b) 10 % CO_2 saturation and crack density of 0.01. The red and blue lines indicate the top and bottom layer reflections respectively.

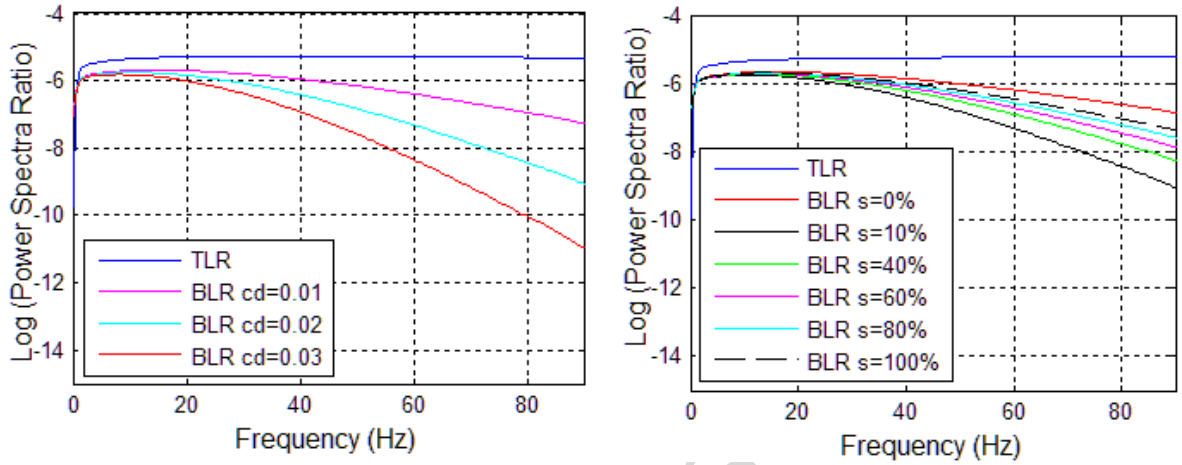

Figure 5: Samples plots of the Log Power Spectral Ratios (LPSR) against frequency at a fixed offset of 1100 m for the third layer (a) 10 % CO_2 saturation at different crack densities (cd) (b) crack density of 0.02 and different percentage of CO_2 saturation (s). TLR is top layer reflection while BLR is bottom layer reflection

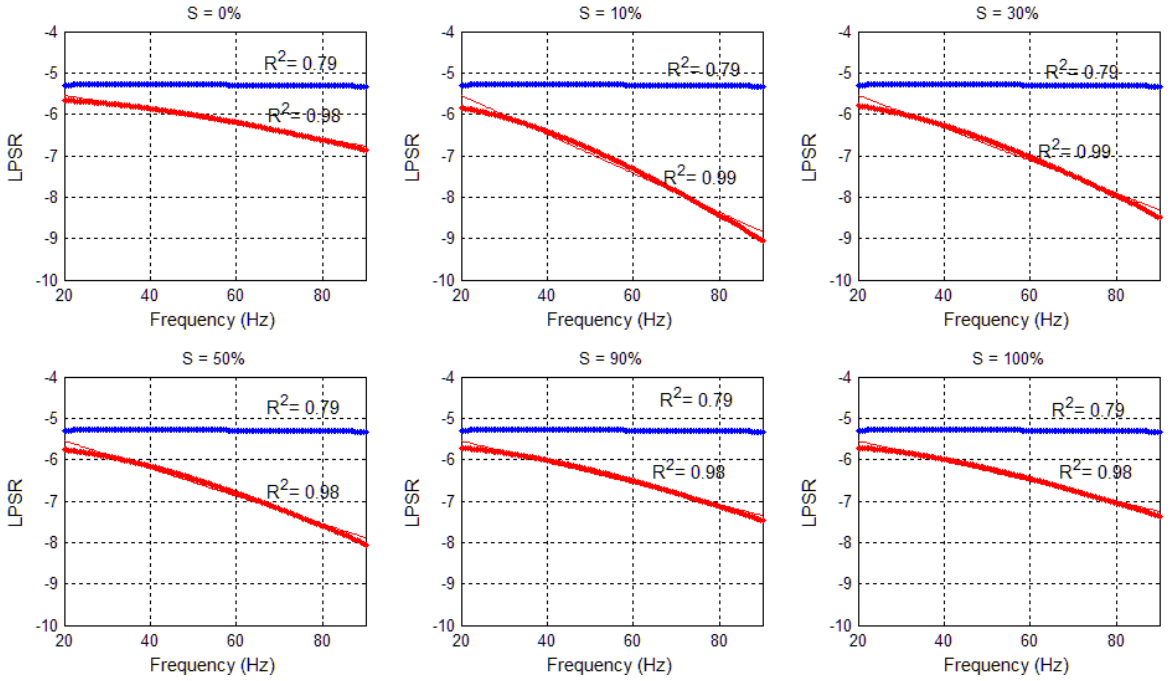

Figure 6: Sample least-squares regression plots for the third layer at a fixed offset of 1100m. The blue colour indicates the top layer reflection while the red colour indicates the bottom layer reflection. S is the degree of saturation of CO_2. The saturation of brine is (100 - S) %.

4.0 Results and analysis

The results of our study demonstrate a strong sensitivity of attenuation to CO_2 saturation. For the pure isotropic model (zero porosity, no microcracks and no fluid saturation), there is no attenuation in the model as expected (pink colour in Figure 7). However, the presence of CO_2

in the model causes attenuation. The induced attenuation depends on the degree of saturation. Higher Q values (low attenuation) are obtained in the fluid-saturated layer at 0% CO_2 saturation and lower Q values (high attenuation) at 100% CO_2 saturation for the three crack densities considered (Figure 7). The Q values are observed to decrease gradually with decreasing percentages of CO_2 saturation from 100% to 10% for a given crack density, implying more attenuation with decreasing percentages of saturation. The Q values are also observed to decrease systematically both with increasing crack density and offset (Figure 7). This implies that the induced P-wave attenuation increases with crack density and offset. Figure 8 shows the attenuation (1/Q) profile against percentages of CO_2 saturation. The attenuation exhibits a non-linear relationship with $C0_2$ saturation. For the ranges of saturations considered, the attenuation peaks at 10% saturation after which there is a gradual and steady decrease in attenuation with increasing percentage of saturation. This gradual decrease appears to be sharper for saturation ranges of around 10 – 50% than higher percentage saturations. A maximum attenuation of up to 0.13 occurs at 10% CO_2 saturation. Although our study is limited only to the effects of crack density and CO_2 saturation, it is useful to show how these factors influence attenuation characteristics to gain a fuller understanding of these effects and gain more confidence in using P-wave attenuation in deciphering information on hydrocarbon fluid properties

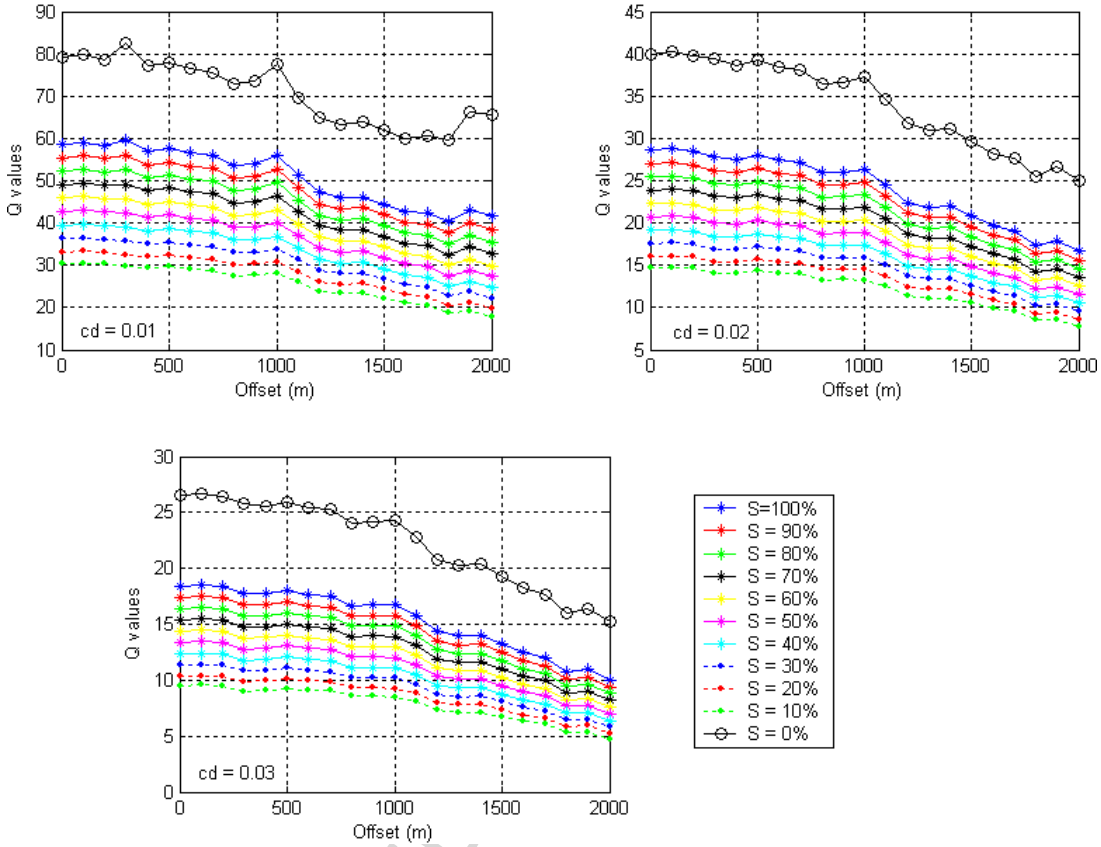

Figure 7: Q profile against CO_2 saturation for different degree of saturations and crack densities. Q decreases systemically with saturation and crack density and is minimum around 10% saturation

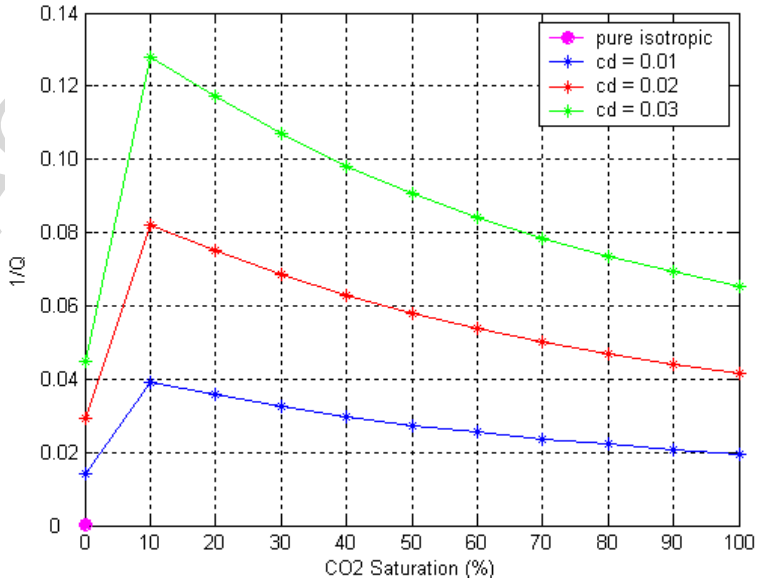

Figure 8: 1/Q profile against CO_2 saturation for different crack densities. No attenuation occurs in the pure isotropic case with no cracks and no fluid saturation (pink colour). The induced attenuation is a maximum at 10% CO_2 saturation.

5.0 Discussion and conclusion

Seismic attenuation depends not only on the physical state of the rocks, but also on the nature of the fluid saturation in the pores of the rock. Based on the mean-field poro-elastic model of Chapman *et al* (2002 and 2003), we have investigated the effects of two types of fluid saturation (brine and CO_2 in the supercritical state) on P-wave attenuation, with particular interest in the effects of CO_2 using the CO_2 properties at the Sleipner gas field in the North Sea. Our results demonstrate the sensitivity of P-wave attenuation to the presence of CO_2. The induced attenuation is influenced by the effective fluid bulk modulus which in turn is dependent on the percentages of saturation of the two fluids (CO_2 and brine). The attenuation is very sensitive to the percentage of CO_2 saturation and is higher for 100% CO_2 saturation than for 0% saturation, implying that the CO_2 causes more attenuation than brine. This could possibly be attributed to the fact that the properties of CO_2 in the supercritical phase where it behaves as a liquid were used in the modelling. Another factor that affects the magnitude of the induced attenuation is the crack density. The attenuation increases with increasing crack density as well as with offset. The attenuation occurs as a result of the relaxation of the fluid-pressure gradients generated by the propagation of seismic waves between the cracks and the surrounding pore space in the rock. The fluid mobility in this case is assumed to be the effective mobility of the two fluids and viscosity effects are not taken into consideration. The results show that the P-wave attenuation is even more sensitive to CO_2 saturation than velocity, most especially at higher concentrations when compared to the results of the study of David *et al* (2008). The attenuation results are also consistent with the results of Rossi *et al* (2011) who demonstrated the sensitivity of attenuation to CO_2 saturation in real field data example from the Sleipner Field. Thus, our findings further demonstrate the sensitivity of attenuation to CO_2 saturation, providing a fuller understanding into attenuation characteristics

in fluid saturated rocks and especially validating the practical utility of using attenuation characteristics as an additional diagnostic in the characterisation of rock formations for a variety of applications, including hydrocarbon exploration and production, subsurface storage of CO_2 or geothermal energy extraction.

Acknowledgement

We are grateful to the Akwa Ibom State University (AKSU) - Nigeria for providing sponsorship to Ekanem's studies at the University of Edinburgh. We also thank all the sponsors of the Edinburgh Anisotropy Project (EAP) for supporting the project and the permission to publish the results.

References

Amir, G and Landro, M., 2009. Estimation of thickness and velocity changes of injected carbon dioxide layers from pre-stack time-lapse seismic data. *Geophysics*, 74(2), 017- 028.

Arts, R., Chadwick, A., Eiken, O., Thibeau, S. and Nooner, S., 2008. Ten years' experience of monitoring CO2 injection in the Utsira Sand at Sleipner, offshore Norway. *First Break*, **26**, 65 - 72.

Arts, R., Eiken, O., Chadwick, A., Zweigel, P., van der Meer, L. and Zinszner, B., 2004. Monitoring of CO2 injected at Sleipner using time-lapse seismic data. *Energy*, **29**, 1383 - 1392.

Bickle, M., Chadwick, A., Huppert, H. E., Hallworth, M. and Lyle, S., 2007. Modelling carbon dioxide accumulation at Sleipner: Implications for underground carbon storage. *Earth and Planetary Science Letters*, **255**, 164 - 176.

Chadwick, R.A., Arts, S. and Eiken, O., 2005. 4D seismic quantification of a growing CO2 plume at Sleipner, North Sea. Petroleum Geology: North-West Europe and Global Perspectives. *Proceedings of the 6th Petroleum Geology Conference*, 1385-1399.

Chadwick, R. A., Williams, G., Delepine, N., Clochard, V., Labat, K., Sturton, S., Buddensiek, M.-L., Dillen, M., Nickel, M., Lima, A. L., Arts, R., Neele, F. and Rossi, G., 2010. Quantitative analysis of time-lapse seismic monitoring data at the Sleipner CO_2 storage operation: *The Leading Edge*, **29**, 170 - 177.

Chapman, M., 2003. Frequency-dependent anisotropy due to meso-scale fractures in the presence of equant porosity. *Geophysical Prospecting*, **51**, 369-379.

Chapman, M. and Liu, E., 2006. Seismic attenuation in rocks saturated with multi-phase fluids. *76th Annual International Meeting, SEG, Extracted Abstracts*, 1988-1992.

Chapman, M., Zatsepin, S. V. and Crampin, S., 2002. Derivation of a microstructural poroelastic model. *Geophysical Journal International*, **151**, 427 - 451.

Chapman, M., Maultzsch, S., Liu, E. and Li, X. Y., 2003. The effect of fluid saturation in an anisotropic multi-scale equant porosity model. *Journal of Applied Geophysics*, **54**, 191 - 202.

Chung, H. and Lawton, D. C., 1995. Frequency characteristics of seismic reflections from thin beds. *Canadian Journal of Exploration Geophysics*, 31, 32-37.

Dasgupta, R. and Clark, R., 1998. Estimation of Q from surface seismic reflection data. *Geophysics*, **63**(6), 2120-2128.

David, L., Don, A., Wright, R., Dave, M. and Cole, S., 2008. Seismic monitoring of CO_2 geo-sequestration: realistic capabilities and limitations. *78th Annual International Meeting, Extracted Abstracts, SEG*, 2841 - 2845.

Davis, T. L., Terrell, M. J., Benson, R. D., Cardona, R., Kendall R. and Winarsky, R., 2003. Multicomponent seismic characterization and monitoring of CO2 flood at Weyburn Field, Saskatchewan. *The Leading Edge,* **22**, 696 - 697.

Eshelby, J. D., 1957. The determination of the elastic field of an ellipsoidal inclusion, and related problem. *Proceedings of the Loyal Society of London*, **A241**, 376 - 396.

Hauge, P.S. 1981. Measurements of attenuation from vertical seismic profiles. *Geophysics* **46**, 1548 -1558.

Johnson, D., Toksoz, M. and Timur, A., 1979. Attenuation of seismic waves in dry and saturated rocks: II. Mechanisms. *Geophysics*, **44**(4): 691 - 711.

Klimentos, T., 1995. Attenuation of P- and S-waves as a method of distinguishing gas and condensate from oil and water. *Geophysics*, **60**, 447 - 458.

Lange, J. N. and Almoghrabi, H. A., 1988. Lithology discrimination for thin layers using wavelet signal parameters. *Geophysics*, **53**(12), 1512-1519.

Lucet, N. and Zinszner, B., 1992. Effects of heterogeneities and anisotropy on sonic and ultrasonic attenuation in rocks. *Geophysics*, **57**, 1018 - 1026.

Maultzsch, S., Chapman, M. Liu, E. and Li, X. Y., 2003. Modelling frequency-dependent seismic anisotropy in fluid-saturated rock with aligned fractures: Implication of fracture size estimation from anisotropic measurements *Geophysical Prospecting*, **51**, 381 - 392.

Maultzsch, S., Chapman, M., Liu, E. and Li, X. Y., 2007. Modelling and analysis of attenuation anisotropy in multi-azimuth VSP data from Clair field. *Geophysical Prospecting,* **55**, 627 - 642.

Mavko, G., Mukerji, T. and Dvorkin, J., 2009. *The Rock Physics Handbook - 2nd edition*. Cambridge University Press.

Murphy, W. F., 1985. Sonic and ultrasonic velocities: Theory versus experiment. *Geophysical Research Letters*, **12**, 85 - 88.

Müller, T. M., Caspari, E., Qi, Q., Rubino, J. G., Velis, D. R., Lopes, S., Lebedev, M., Gurevich, B., 2015. Acoustics of Partially Saturated Rocks: Theory and Experiments: in "Seismic Exploration of Hydrocarbons in Heterogeneous Reservoirs: New Theories, Methods and Applications", 370 pages, p. 45 - 76.

Pujol J. and Smithson S. 1991. Seismic wave attenuation in volcanic rocks from VSP experiments. *Geophysics* **56**, 1441 - 1455.

Roberts, J., 2009. Developing the Rock Physics Model - Improved Carbon Dioxide Mixing Rules for Carbon Capture and Storage. *71st Conference & Technical Exhibition, EAGE*, Expanded Abstract.

Rossi G., Chadwick R.A. and Williams G.A., 2011. Traveltime and Attenuation Tomography of CO2 Plume at Sleipner. 7*3rd Conference & Technical Exhibition, EAGE*, Expanded Abstract.

Rubino, J.G., Velis, D. R. and Sacchi, M. D., 2011a. Numerical analysis of wave-induced fluid flow effects on seismic data: Application to monitoring of CO2 storage at the Sleipner Field, *J. Geophys. Res*., 116, B03306.

Rubino, J. G. and Velis, D. R., 2011b. Seismic characterization of thin beds containing patchy carbon dioxide-brine distributions: A study based on numerical simulations, *Geophysics*, 76, 3, R57 - R67.

Sothcott, J., McCann, C. and O'Hara, S., 2000. The influence of two pore fluids on the acoustic properties of reservoir sandstones at sonic and ultrasonic frequencies. *70th Annual International Meeting, SEG, Expanded Abstracts*, 1883 - 1886.

Taylor, D., 2001. *ANISEIS v5.2 Manual*. Applied Geophysical Software Inc., Houston.

Toksõz, M. N. Johnston, D. H. and Timur, A., 1979. Attenuation of seismic waves in dry and saturated rocks: I. Laboratory measurements: *Geophysics*, **44**, 681 - 690.

White, J. E., 1975. Computed seismic speeds and attenuation in rocks with partial gas saturation. *Geophysics*, **40**(2), 224 - 232.

Winkler, K.W., 1986. Estimates of velocity dispersion between seismic and ultrasonic frequencies. *Geophysics*, **51**, 183 - 189.

Winkler, K. W. and Nur, A., 1982. Seismic attenuation: effects of pore fluids and frictional sliding. *Geophysics*, **47**, 1 - 15.

Highlights

Used poro-elastic model to examine effect of CO_2 on P-wave attenuation

P-wave attenuation is sensitive to CO_2 saturation

Attenuation increases with decreasing percentage of CO_2 saturation

P-wave attenuation is sensitive to crack density and offset

CO_2 causes more attenuation than brine